E-MRS Spring Meeting 2015 Symposium C - Advanced inorganic materials and structures for photovoltaics

Realistic simulation of metal nanoparticles on solar cells

F.Cortés-Juan[a,b*], Alba Espinosa-Soria[a], J.P.Connolly[a], Guillermo Sánchez-Plaza[a], J.P.Hugonin[c], P.Sanchis[a]

[a] Valencia Nanophotonics Technology Center, Ed 8F Camino de Vera s/n 46022 Valencia. Spain
[b] Laboratoire de Photonique et Nanostructures (LPN-CNRS), Route de Nozay, 91460 Marcoussis, France
[c] Institut d'Optique, CNRS, Université Paris-Sud 11, 2, Avenue Augustin Fresnel, 91127 Palaiseau Cedex, France

Abstract

We present a strategy for simulating the scattering effect of an array of self-aggregated (SA) metal nanoparticles (NPs) on the light absorption in solar cells. We include size and shape effects of the NPs, the effect of a layered substrate and the effect of the interaction between NPs. The simulation relies on realistic characterization by SEM microscopy of the random NP arrays. Time and memory limitations of numerical approaches are overcome using semianalytical expressions. Size and shape considerations deal with truncated-sphere shapes by using a polarisability tensor. This is a development of other models leading to equivalent dipoles from the external source and the radiated fields from the rest of NPs. Once an equivalent array of 3-D dipoles is found, the total electromagnetic field and optical simulations are performed. The general trends show good agreement with experimental measurements. A critical analysis of the model is presented, and some improvement strategies are discussed for future studies.

1. Introduction

The majority of solar cell technologies are currently based on Si, as the industry is still focused on Si-based processes. However, as other minor technologies are increasing its efficiency most industrials look for a competitive

* Corresponding author. Tel.: +34-963-877-000 (Ext.88110); fax: +34-963-877-827.
  E-mail address: frecorju@ntc.upv.es

advantage by reducing costs while maintaining high efficiency. In Si photovoltaics, up to 51% of the cost is due to the silicon wafer, so a thickness reduction of the cells is therefore planned in the next years [1].

However, this thickness reduction leads to incomplete light absorption. Thinner solar cells therefore require light trapping strategies different from the traditional texturing, as textured thinner solar cells are expected to have a much greater breaking ratio during production.

A solution is possible with the use of nanostructures which provide scattering and therefore an enhancement in light absorption. Moreover some techniques, such the self-aggregation, have already been demonstrated to be economically feasible from the industrial point of view in the photovoltaic industry [2].

The self-aggregation method lead to nanoparticles that are not completely spherical or spheroidal [3], but rather truncated forms. This is intrinsic to the fabrication process and the wetting properties of the materials involved. Thus, traditional spherical models based on Mie seem not so appropriated to predict the behaviour of those systems, and the final application makes the multi-layered substrate too important to neglect its effect.

This work presents an approach to simulate the behaviour of metal nanoparticles over a stratified media assuming truncated spheres and a dipole-like radiation system solved using Green's function techniques. Thus, in Section 2 the details of a semianalytical model to obtain the polarisability of truncated spheres are presented, together with a critical analysis of its numerical particularities and the results. In section 3, the strategy in the use of Green functions to solve the induced dipoles is presented, taking as the exciting source not only the external exciting field but also the field radiated by the rest of the nanoparticles/dipoles. The model is tested in Section 4, where a critical comparison between experimental and simulated data is performed.

Nomenclature

|	
NP	Nanoparticle
SA	Self-aggregated
α_H	Parallel or horizontal eigenpolarisability
α_V	Normal or vertical eigenpolarisability
α	Polarisability tensor
R	Radius of the spherical nanoparticle
a	Radius of the theoretical intersection between the spherical nanoparticle and the substrate
θ	Truncation angle
ε	Permittivity function of a material
V	Volume of a nanoparticle of radius R
$V_{a=1}$	Volume of a truncated nanoparticle in Jesper-Jung's model
$K_{H,V}$	Integral Kernels (Parallel and Vertical, respectively)
N	degree of the Laguerre polynomial / degree of Gauss-Laguerre quadrature
z_j	j^{th} zero of the Laguerre Polynomial of degree N
ω_j	j^{th} weighting factor for the Gauss-Laguerre quadrature
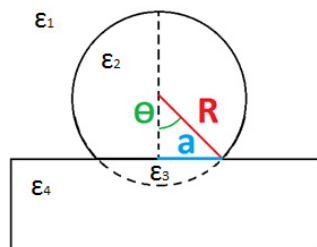
Figure 1 Schema of the structure studied by Jesper Jung. Three different materials can be considered in four different regions, corresponding to the substrate (4 or 3-4), the nanoparticle (2-3 or 2) and the surrounding upwards media (1, usually air). The truncation angle is defined from the bottom of the particle. All the solutions are calculated assuming that the parameter "a" is kept constant to 1.

2. Polarisability of truncated nanoparticles

There are many references dealing on how to model the polarisability of spheres [4] and spheroids [5]. However, only a few take the substrate into account, even if its effect, when thinking on a solar cell application, is too important to neglect.

One of the simplest ways to take the substrate into account is defining an average or effective refractive index [6]. Other more precise models deal with an imaginary source to take into account the reflected power from the substrate (the image dipole approximation [7]). Some variants of those have proposed to include the effect of the image dipole into a more complex definition of the effective refractive index of the surrounding media [8].

One of the most suitable models and expressions for calculating the polarisability of a truncated nanoparticle on a substrate can be found in Bedeaux and Viegler [9]. This is one of the more accurate analytical expressions dealing with self-aggregated nanoparticles. However, there are some simplifications that lead to similar results, such as Jesper Jung's approach [10].

In this paper, Jesper Jung's approach is used and analysed. This model is based on the quasi-static approximation (QSA), so it neglects any retardation effect and thus will be only valid for small nanoparticles. This limitation can easily be overcome by the right choice of the nanoparticle distribution. The QSA approach has its advantages as it makes independent the geometrical influence of the nanoparticle from the properties of the involved materials. This allows the mathematical treatment to be simplified and analytical solutions are possible even for complex geometries. This makes the QSA an interesting approach for the geometries involved in this work. The structure modelled by Jesper Jung is shown in Fig. 1.

In summary, Jensen Jung uses toroidal coordinates to solve the electrostatic potential of a truncated sphere. By comparing some of the expressions during its mathematical development, he is able to define two directional eigenpolarisabilities: The first one horizontal or parallel to the substrate (α_H) and the second one vertical or normal to it (α_V). This two eigenpolarisabilities imply that, for normal incidence of light, the main axis of the polarisation correspond to the main axis of the eigenpolarisability. Thus, the main condition that Bohren-Huffman required [11] to properly define a polarisability tensor is required, leading to eq.1:

$$\boldsymbol{\alpha} = \begin{pmatrix} \alpha_H & 0 & 0 \\ 0 & \alpha_H & 0 \\ 0 & 0 & \alpha_V \end{pmatrix} \tag{1}$$

The full details of the model can be found in the original reference [10]. Here, only some comments and a brief analysis of the model is presented:

First, the geometrical influence of the truncation angle is expressed in two-parameter integral Kernels: For each truncation angle θ there is one used to obtain the parallel eigenpolarisability $K_H(x,y,\theta)$ and another for the perpendicular one $K_V(x,y,\theta)$. Second, the eigenpolarisabilities are found by solving a Fredholm's integral equation of second kind (eq.2). In order to solve it matricially, a Gauss-Laguerre Quadrature can be performed, leading to eq.3

$$\boldsymbol{b}(\mu,\theta,\lambda) + \boldsymbol{A}^{-1}(\mu,\theta,\lambda) \int_0^\infty \boldsymbol{H}(\mu,\gamma,\theta,\lambda)\, \boldsymbol{b}(\gamma,\theta,\lambda)d\gamma = \boldsymbol{A}^{-1}\boldsymbol{f}(\mu,\theta,\lambda) \tag{2}$$

$$\boldsymbol{b}(\mu,\theta,\lambda) + \boldsymbol{A}^{-1}(\mu,\theta,\lambda) \sum_{j=1}^{N} \boldsymbol{H}(\mu,z_j,\theta,\lambda)\, \boldsymbol{b}(z_j,\theta,\lambda)\omega(z_j) = \boldsymbol{A}^{-1}(\mu,\theta,\lambda)\boldsymbol{f}(\mu,\theta,\lambda) \tag{3}$$

In eq.2 and eq.3 the matrix **H** includes the Kernel values. Therefore different values of **H** (and thus different values for the solution vector **b**) will be obtained depending on the choice of the eigenpolarisability (parallel or normal). Moreover, the matrix **A** is very badly conditioned as the toroidal coordinates involve hyperbolic trigonometrical functions that lead to very big and very small values at the same time. Thus, it becomes numerically singular for parameters beyond μ=10.

This implicitly defines the maximum possible order of the Gauss-Laguerre quadrature as the greater zero of the 4th degree Laguerre Polynomial is about 9.6 whereas for the 5th degree is beyond 10. Thus, the quadrature should

be done for N=4. An alternative would be to use symbolic variables to invert analytically the **A** matrix and then substitute the values. This is feasible for a 4x4 matrix. However, during the final matrix inversion to solve the system in eq.4, similar problems occur and no analytical expression is found for inverting a 4Nx4N symbolic matrix for N≥4. Even if the inversion is avoided using other strategies such like the LU decomposition, the numerical problems of using μ>10 seem to be unavoidable. Equation 3 can be solved matricially making all μ_j parameters correspond to a z_j. For each truncation angle and wavelength:

$$\begin{pmatrix} \boldsymbol{A}^{-1}(z_1)\boldsymbol{H}(z_1,z_1)\omega(z_1)+\boldsymbol{Id_{4x4}} & \cdots & \boldsymbol{A}^{-1}(z_1)\boldsymbol{H}(z_1,z_N)\omega(z_N) \\ \vdots & \ddots & \vdots \\ \boldsymbol{A}^{-1}(z_N)\boldsymbol{H}(z_N,z_1)\omega(z_1) & \cdots & \boldsymbol{A}^{-1}(z_N)\boldsymbol{H}(z_N,z_N)\omega(z_N)+\boldsymbol{Id_{4x4}} \end{pmatrix}\begin{pmatrix} \boldsymbol{b}(z_1) \\ \vdots \\ \boldsymbol{b}(z_N) \end{pmatrix}=\begin{pmatrix} \boldsymbol{A}^{-1}(z_1)\boldsymbol{f}(z_1) \\ \vdots \\ \boldsymbol{A}^{-1}(z_N)\boldsymbol{f}(z_1) \end{pmatrix} \quad (4)$$

Once the **b** vector is solved in eq.4 for $\mu_j=z_j$, eq.3 can be used to solve b for many other values of μ. With those, the eigenpolarisabilities are found as:

$$\propto_H = 8\pi \int_0^\infty \mu b_H(\mu)d\mu \quad (5)$$

$$\propto_V = 8\pi \int_0^\infty (1+\mu^2)b_V(\mu)d\mu \quad (6)$$

Where b_H and b_V values correspond to some of the **b** elements depending on the Kernel choice in matrix **H** (eq.3). Notice that those improper integrals can be solved again with a Gauss-Laguerre Quadrature with the advantage of using the same abscissas and weighting factors that have been previously calculated for solving the b(μ) values in eq.4. This will avoid using eq.3 recursively.

A latter comment on this model is related with how to transform the eigenpolarisabilities in the actual polarisabilities. The model obtains α_H and α_V in terms of volume units. Thus, the correction factor is:

$$\propto \left[\frac{Cm^2}{V}\right] = 4\pi\epsilon \frac{V}{V_{a=1}} \propto [m^3] \quad (7)$$

Notice that, for any truncation angle, the solution corresponds to a truncated particle whose theoretical intersection with the substrate always define a circle with radius a=1 (see Fig.1). This means that the radius of the particle increases as the truncation angle decreases.

Fig.2a and Fig.2c show that as the truncation angle increases, an important redshift is found for the resonance of the parallel polarizability, whereas a slight blueshift occurs for the vertical one (Fig.2b and 2d). This is consistent with the flattened particles behaviour, as when increasing the aspect ratio the longer axis supports lower energy resonances and the short axis supports higher ones. The smaller difference in the blueshifted resonances is mainly due to the differences between the wavelength and the energy scales.

Moreover, both polarisabilities decrease with the truncation angle as the particles become smaller in volume and thus there are less charges to be polarised. However, the vertical polarizability decreases faster than the parallel as the Feret diameter in the vertical axis always decreases with increasing truncation angles and this is not true for the parallel direction. This dimensional comparison in terms of the Feret Diameter also explains why the redshift is even more important at truncation angles beyond 90degrees.

In brief, as shown in Fig.2, even if the quadrature is limited to N=4, the resulting eigenpolarisabilities for a Ag nanoparticle on a silicon oxide substrate show a resonance that fits with the expected behaviour at increasing truncation angles. Moreover, the Mie theory predicts a polarizability for spherical Ag nanoparticles in the range of 10^{-31}-10^{-33} C·m/V. However, the exact values may not be too accurate as there are several quadratures involved and because their accuracy is limited by the numerical issues that have been described.

3. Determination of equivalent dipoles using Green functions

The standard strategy when studying radiating nanoparticles is to substitute the nanoparticle itself by an equivalent radiating source. In this case only dipoles are going to be considered, as higher excitation orders usually appear at much higher sizes.
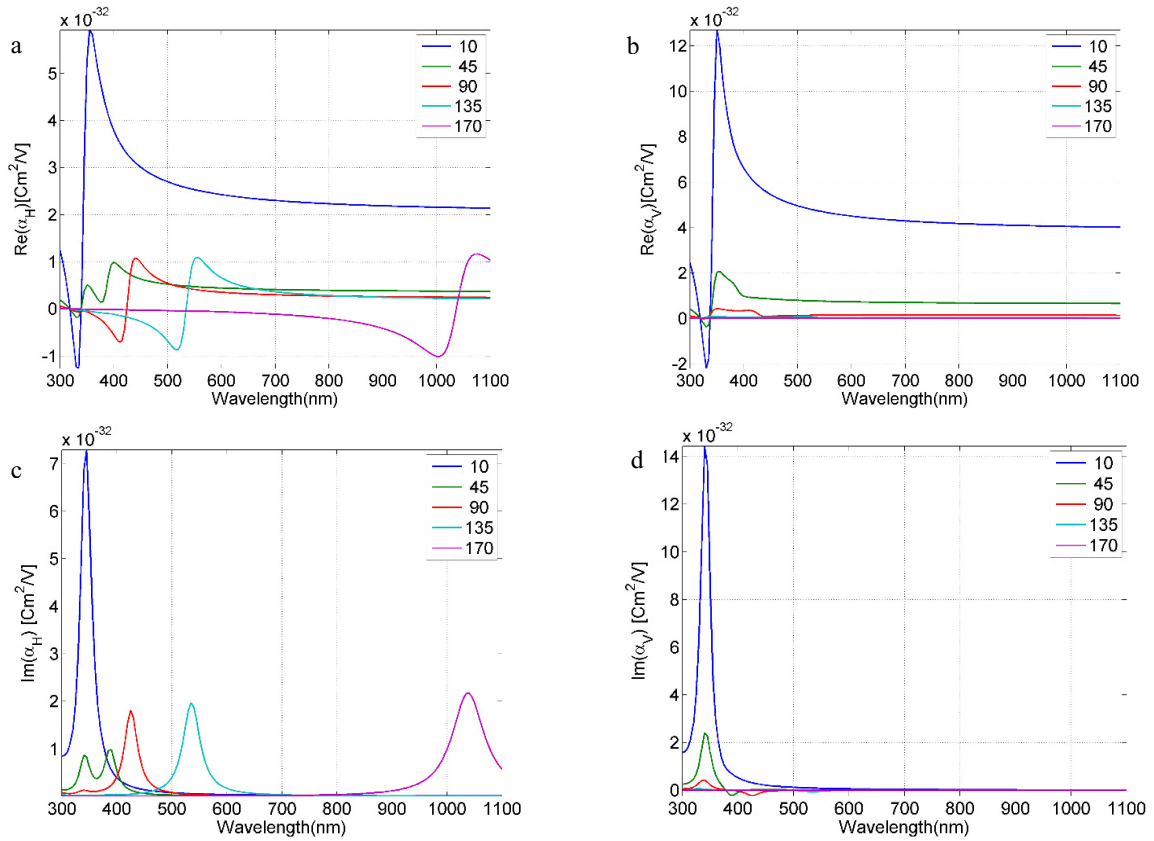
Figure 2 Normal components of the polarisability values for truncated spheres of 10nm of radius. The different curves correspond to different truncation angles (in degrees). Left column corresponds to the real part (a) and the imaginary part (c) of the parallel to de interface component. Right column corresponds to the real part (b) and the imaginary part (d) of the parallel to de interface component.

Thus, the equivalent dipoles have to be determined. The tensor polarisability has already been calculated with the Jesper Jung approach. Now, the external exciting electric field has to be calculated. In order to do this, both the external source of light and the radiated fields by the rest of the nanoparticles are necessary to find the radiated field by a nanoparticle. Thus, there is an implicit dependence that would need a complex iterative method to solve the whole system. However, there is another way that allows to solve the problem matricially: The Green Functions. In short, when a Green Function is used, the radiated field for a single isolated nanoparticle reduces to:

$$\boldsymbol{E}_R(x_2, y_2, z_2) = \boldsymbol{G}(x_2, y_2, z_2, x_1, y_1, z_1) \cdot \boldsymbol{P}(x_1, y_1, z_1) = \boldsymbol{G}(x_2, y_2, z_2, x_1, y_1, z_1) \cdot \alpha \cdot \boldsymbol{E}_0(x_1, y_1, z_1)$$
(8)

The radiated field of a nanoparticle i in a M-nanoparticle array then becomes:

$$\boldsymbol{P}_i(x_i, y_i, z_i) = \alpha_i \cdot \boldsymbol{E}_T(x_i, y_i, z_i) = \alpha_i \cdot \left(\boldsymbol{E}_0(x_i, y_i, z_i) + \sum_{\substack{j=1 \\ i \neq j}}^{M} \boldsymbol{G}(x_i, y_i, z_i, x_j, y_j, z_j) \, \boldsymbol{P}_i(x_i, y_i, z_i) \right)$$
(9)

From equation 9, it is possible to solve all the dipoles at once:

$$\begin{pmatrix} P_1 \\ P_2 \\ \vdots \\ P_M \end{pmatrix} = \begin{bmatrix} Id_{3Mx3M} - \begin{pmatrix} 0_{3x3} & G_{21} & \cdots & G_{M1} \\ G_{12} & 0_{3x3} & \cdots & G_{M2} \\ \vdots & \vdots & \ddots & \vdots \\ G_{1M} & G_{2M} & \cdots & 0_{3x3} \end{pmatrix} \end{bmatrix}^{-1} \cdot \begin{pmatrix} \alpha_1 Id_{3x3} & 0_{3x3} & \cdots & 0_{3x3} \\ 0_{3x3} & \alpha_2 Id_{3x3} & \cdots & 0_{3x3} \\ \vdots & \vdots & \ddots & \vdots \\ 0_{3x3} & 0_{3x3} & \cdots & \alpha_N Id_{3x3} \end{pmatrix} \cdot \begin{pmatrix} E_0 \\ E_0 \\ \vdots \\ E_0 \end{pmatrix} \quad (10)$$

In eq.10, for simplicity, the dependency on the spacial coordinates has been removed. The G_{ji} are the 3x3 Dyadic Green Functions that express the radiated field from the particle j to the particle i. It has been assumed that the external electric field corresponds to an infinite plane wave, so every particle is externally excited in the same way. Notice that eq.10 is still valid even if the polarisabilities α_i are 3x3 tensors $\boldsymbol{\alpha_i}$ as shown in eq.1.

The Green function for an elementary dipole in a homogeneous medium is well known [12]. When a substrate is taken into account, some differences have to be included in the Green Functions as well as in eq.10, as the particle can interact with itself (just like the image-dipole approximation proposes). Thus, instead of having an Id_{3Nx3N} in equation 10, another Green function should be included.

Fortunately, the radiation problem over a two layered substrate has already been solved so the expressions for those Green functions are also known. They are too complex to be summarized here, but they can be found elsewhere [13]. The main difference is that a tensor polarisability $\boldsymbol{\alpha}$ will be used instead of a scalar value α.

In this approach, thus, point dipoles will be considered placed at the centre of the nanoparticles. This dimensional assumption implies that the solution will not be realistic within the space actually occupied by the nanoparticles, but everywhere else it will be correct [11].

4. Testing the model

The experimental validation of the model is not easy as transmission measurements are not feasible on a 180μm c-Si substrate in the visible range and only reflection measurements can be done.

The model allows to define the radiating sources at any point in the space. Thus, it is possible to make real random distributions by taking SEM images and analysing the particles using a software like ImageJ (Fig.3b). In Fig.3a, a real NPs self-aggregated nanoparticle distribution is shown. In this case, a 3nm Ag precursor layer is deposited on 65nm of SiO$_x$ antireflection coatings on Si and then annealed 1h at 200º under inert conditions.

In Fig.3 it is possible to see that even if the particles are not perfectly spherical from above, this approach seems reasonable. Indeed, making statistics from different SEM images with a total of 1964 analysed NPs, it is found that the average circularity (Fig.3c) is of 0,906±0.001. Moreover, the average size of the nanoparticles (Fig.3d) is of R=9,8±0,1 nm, small enough to be able to use with the quasi-static approximation. For the truncation angle, the measurement is much more difficult to perform as the SEM images are not easy to take. Moreover this image treatment requires an important manual work. As most images show angles between 45 and 90 degrees, a random distribution of angles between these two limits will be used.

With these data and using the Green functions, a mapping of the electromagnetic field is done. This allows to calculate the absorption losses within the nanoparticle as well as the flux of the Poynting vector. Thus, optical magnitudes like reflectivity, transmission and absorption can be obtained, as shown in Fig.4.

The induced currents in the Ag NPs lead not only to a radiating dipole but to ohmic losses (red curve in Fig.4). Thus, at the wavelength range at which the scattering peak is placed (around 400nm), the absorption of light by the silicon substrate is reduced (black curve). All this has already been verified experimentally in finished solar cells by measuring internal quantum efficiency [14].

However, even if the overall trends correspond with the expected results, when comparing values the model shows important differences (Fig.5). The Green Functions used in this paper have already been tested and verified in [15]. Thus, there are different possible reasons for the discrepancies between experimental and modelled results:

4.1. The error in the determination of polarisability values

These error come from the determination of polarisability values, due to all the numerical issues explained in Section 2. In order to verify this, as the main differences can be seen for the horizontal polarisability, the scattering of equivalent truncated spheres have been modelled numerically using CST-Studio Suite (Fig.6).
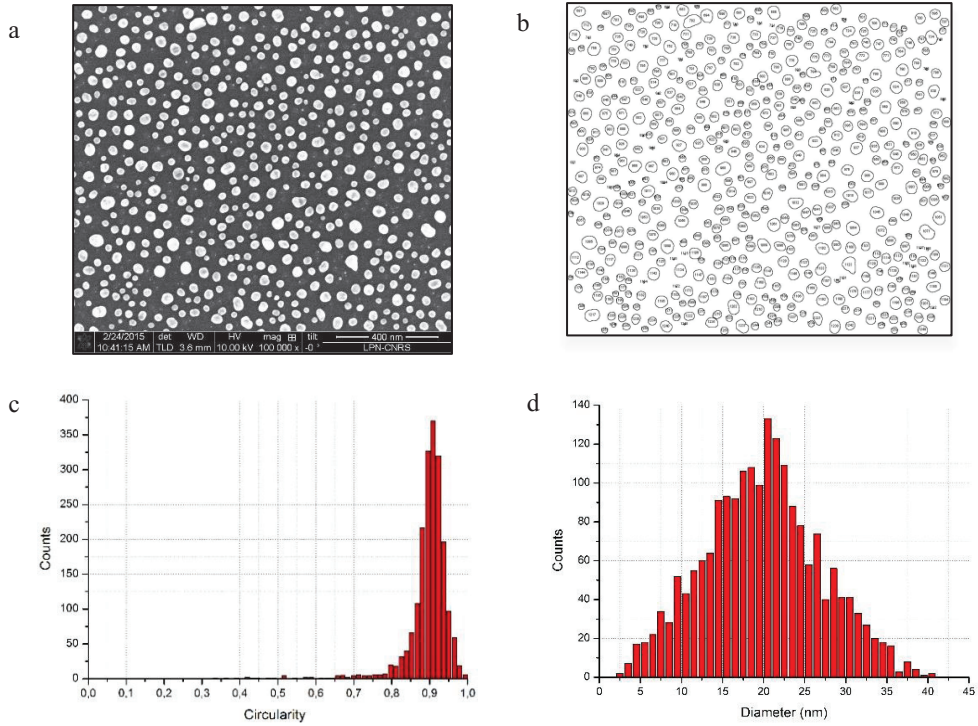
Figure 3 (a) SEM image of a self-aggregated Ag array of NPs. (b) Treated image with particle recognition of the simple using ImageJ (c) Circularity of the NPs shape (d) Size distribution of the array assuming circular particles.
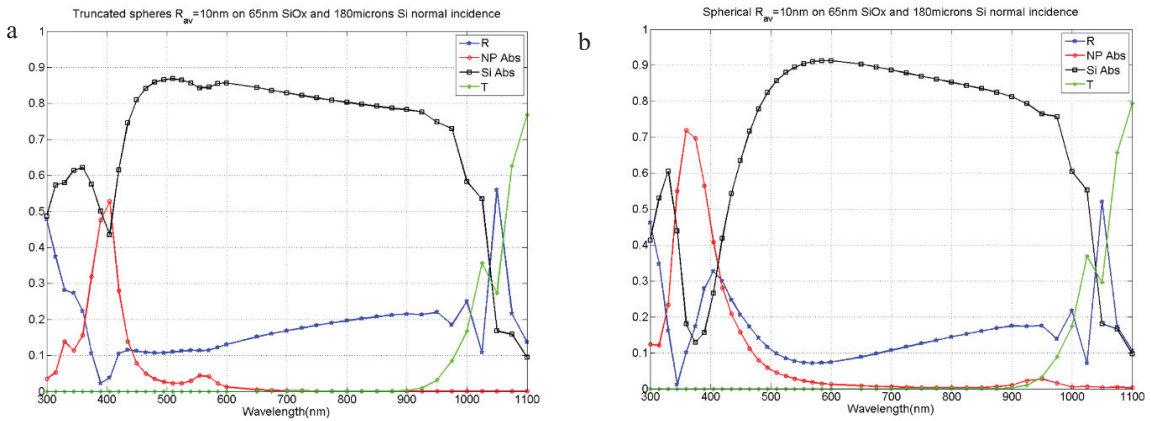

Figure 4 Simulation results for truncated spheres (a) and spheres (b), both of average radius of 10nm on 65nmSiOx and 180µm of polished silicon. Reflexion (R), transmission though the substrate (T), absorption within the silicon substrate (Si Abs) and absorption losses within the nanoparticles (NP Abs) are shown.
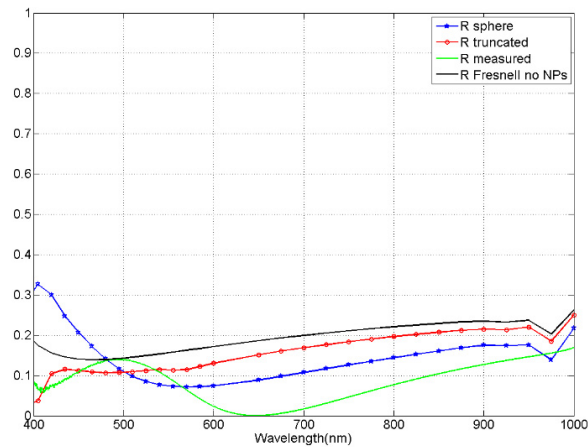
Figure 5 Comparison of the measured reflectivity (green line), the calculated reflectivity of the ARC without NPs using Fresnel Equations (black line), the calculated reflectivity assuming truncated nanoparticles (red line) and assuming spherical nanoparticles (blue line).
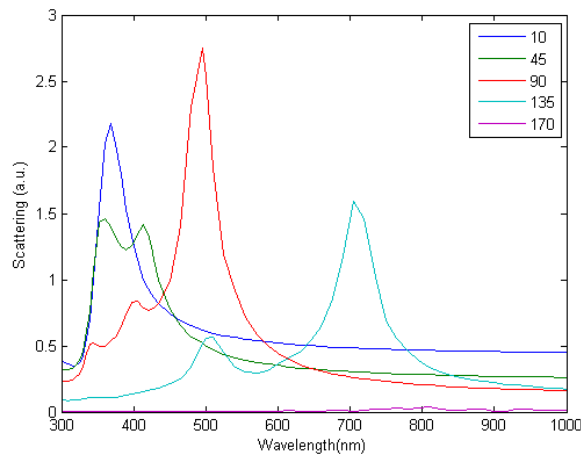

Figure 6 Numerical solution for the scattering spectra of a truncated Ag NP on a 65nm-185µm SiO$_2$/Si substrate, with normal incident light.

By using a numerical software such as CST, an accurate solution is found and it is possible to shed light on the real consequences of the QSA assumptions. In Fig.6 it is shown that the trends seen in Fig.2 are correct. However, the numerical solution is redshifted when compared with the analytical one. This points towards retardation effects that are completely neglected by the electrostatic approximation. Another consequence of these retardation effects is the appearance of different excitation modes, as seen in Fig.6 with the multiple scattering maxima for each curve. The presence of those modes, probably quadrupoles, should be included in further studies for better results. Therefore, even if Mie model predicts that the main contribution for scattering for Ag NPs under 80nm at visible frequencies is due to a dipole, and even if this is even more exact at smaller sizes, the presence of a substrate lead to completely different results.

4.2. The plasmon hybridization

This occurs when particles are very close one to the other. The hybridization term is used to make a parallelism with the hybridization of atomic orbitals when two atoms interact [16]. In the same way, there is a splitting in the resonance energies leading, in a general way, to non-radiating (dark) more energetic resonance modes (thus, with

huge ohmic losses), and to radiating (bright) less energetic resonance modes. However, for a randomly distributed model it is not easy to include these effects.
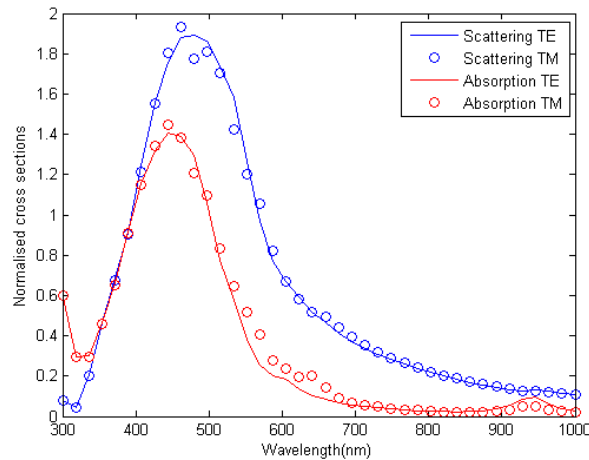

Figure 7 Normalised scattering (blue) and absorption (red) cross sections for a spherical array of NPs equivalent to Fig.2a in a homogeneous medium of refractive index of 1.5. Different curves correspond to different excitation polarisations: TE (line) and TM (dot).

As a first approach, the scattering and absorption cross sections of the array showed in Fig.2 are performed with MATLAB, using a slightly modified version of Mackwoski's MSTM code [17]. The results are in Fig.7, where it is shown that for both polarisations the results are quite similar, both in scattering and in absorption. This behaviour is typical of independent spherical nanoparticles, so these results point towards a very low global interaction between them. There are, however, two remarks to be done: First, as the curves show the overall scattering, any interaction effect leading to a split in energy would be minimised in the global scattering. This means that the small differences between TE and TM modes (around 480nm for scattering and about 650nm for absorption) can be understood as interacting nanoparticles but in a very small fraction. Second, further studies should be done to obtain robust conclusions when the substrate is included as it has already been demonstrated the strong effect that the substrate has.

4.3. The Fano resonances

Another consequence of the presence of multiple particles, apart from the plasmon hybridization, is the interaction between excitation modes that lead to Fano resonances in the optical field. In brief, the Fano interference comes when a bright mode interacts with a dark mode [18]. This is the most difficult aspect to take into account, but for randomly distributed nanoparticles, theoretical calculations show it is likely to find both bright and dark excitation modes [19]. Moreover, previous studies show that even the presence of a substrate can induce Fano resonances [20]. Looking at Fig.5 no clear asymmetric lineshape is found (typical for Fano resonances), but the presence of a zero reflectivity near 650nm can be a clue.

5. Conclusions

In this paper, a critical analysis on a semi-analytical model to obtain the polarisabilites of truncated spheres on multi-layered substrates is done. Then, the model has been applied to simulate a random array of Ag nanoparticles over a substrate together with Green functions that solve matricially all the induced dipoles. Once the equivalent dipoles are known the overall radiated field is obtained. The overall trends related with the optical properties on scattering, absorption in the Si and overall transmission are satisfactory. However, there is an important mismatch when comparing values. The first numerical verifications suggest that the presence of a substrate and the truncation lead to a redshift in the expected resonant frequencies as well as to higher order excitation modes that should be

included for more accurate results. Mie model is no longer valid here due to the inhomogeneity of the medium, and purely numerical modelling may be needed for that purpose.

The analysis is completed with some hypothesis that should be verified in future studies and that are related with the array configuration: The plasmon hybridization and the Fano resonances. The study of both phenomena would shed some light on the origin of the ohmic losses within the NPs, giving a chance to find a way to reduce them.

Acknowledgements

References

[1] ITRPV Edition 2015. International Technology Roadmap for Photovoltaic (ITRPV.net) 2014 Results.   (April 2015).
[2] Vázquez,M.A., et al. "Cost model developed in European project LIMA". Energy Procedia 27 (2012). 646-651.
[3] J.P. Connolly et al. "Analysis of Plasmonic Nanoparticle Fabrication Techniques for Efficient Integration in Photovoltaic Devices" 25th EUPVSEC. pp.773-776 (2010)
[4] Wiscombe, Warren J. "Improved Mie scattering algorithms." Applied optics 19.9 (1980): 1505-1509.
[5] Shoji Asano and Giichi Yamamoto, "Light Scattering by a Spheroidal Particle," Appl. Opt. 14, 29-49 (1975)
[6] Grzela, Grzegorz, Djamila Hourlier, and Jaime Gómez Rivas. "Polarization-dependent light extinction in ensembles of polydisperse vertical semiconductor nanowires: A Mie scattering effective medium." Physical Review B 86.4 (2012): 045305.
[7] Marc A. Taubenblatt and Tuyen K. Tran, "Calculation of light scattering from particles and structures on a surface by the coupled-dipole method," J. Opt. Soc. Am. A 10, 912-919 (1993)
[8] Vernon, Kristy C., et al. "Influence of Particle− Substrate Interaction on Localized Plasmon Resonances." Nano letters 10.6 (2010): 2080-2086.
[9] D. Bedeaux and J. Vlieger, "Optical Properties of Surfaces". Imperial College Press (2004)
[10] J. Jung, T. G. Pedersen, "Polarizability of supported metal nanoparticles: Mehler-Fock approach". Journal of Applied Physics 09/2012 112(6). DOI: 10.1063/1.4752427
[11] C.F. Bohren and D.R. Huffman "Absorption and Scattering of Light by Small Particles". Wiley-VCH, 2004. pp.150
[12] Fung, Kin Hung, and C. T. Chan. "Analytical study of the plasmonic modes of a metal nanoparticle circular array." Physical Review B 77.20 (2008): 205423
[13] L.Novotny, "Allowed and forbidden light in near-field optics. I. A single dipolar light source". Journal of the Optical Society of America A, 14(1), pp.91-104.
[14] F. Cortés-Juan et al., "Plasmonic Nanoparticle Integration with Si Back Contact Solar Cells", 28th EUPVSEC pp.375-379.
[15] M. Langlais et al., "Cooperative electromagnetic interactions between nanoparticles for solar energy harvesting." Optics express 22.103 (2014): A577-A588.
[16] Prodan.E, et al. "A hybridization model for the Plasmon Response of Complex Nanostructures". Science 17 October 2003:302 (5644) 419-422. DOI: 10.1126/science.1089171
[17] Mackowski, D. W., and M. I. Mishchenko. "A multiple sphere T-matrix Fortran code for use on parallel computer clusters." Journal of Quantitative Spectroscopy and Radiative Transfer 112.13 (2011): 2182-2192.
[18] Joe, Yong S., Arkady M. Satanin, and Chang Sub Kim. "Classical analogy of Fano resonances." Physica Scripta 74.2 (2006): 259.
[19] Stockman, Mark I., Sergey V. Faleev, and David J. Bergman. "Localization versus delocalization of surface plasmons in nanosystems: can one state have both characteristics?." Physical review letters 87.16 (2001): 167401.
[20] Zhang, Shunping, et al. "Substrate-induced Fano resonances of a plasmonic nanocube: a route to increased-sensitivity localized surface plasmon resonance sensors revealed." Nano letters 11.4 (2011): 1657-1663.